SCIENCE CHINA
Earth Sciences

• RESEARCH PAPER •

March 2016 Vol.59 No.3: 484–494
doi: 10.1007/s11430-015-5187-2

Ocean satellite data assimilation experiments in FIO-ESM using ensemble adjustment Kalman filter

CHEN Hui[1,2], YIN XunQiang[1,2], BAO Ying[1,2] & QIAO FangLi[1,2*]

[1] *The First Institute of Oceanography, State Oceanic Administration, Qingdao 266061, China;*
[2] *Key Laboratory of Marine Science and Numerical Modeling, State Oceanic Administration, Qingdao 266061, China*

Received February 20, 2015; accepted June 23, 2015; published online November 26, 2015

Abstract Using Ensemble Adjustment Kalman Filter (EAKF), two types of ocean satellite datasets were assimilated into the First Institute of Oceanography Earth System Model (FIO-ESM), v1.0. One control experiment without data assimilation and four assimilation experiments were conducted. All the experiments were ensemble runs for 1-year period and each ensemble started from different initial conditions. One assimilation experiment was designed to assimilate sea level anomaly (SLA); another, to assimilate sea surface temperature (SST); and the other two assimilation experiments were designed to assimilate both SLA and SST but in different orders. To examine the effects of data assimilation, all the results were compared with an objective analysis dataset of EN3. Different from the ocean model without coupling, the momentum and heat fluxes were calculated via air-sea coupling in FIO-ESM, which makes the relations among variables closer to the reality. The outputs after the assimilation of satellite data were improved on the whole, especially at depth shallower than 1000 m. The effects due to the assimilation of different kinds of satellite datasets were somewhat different. The improvement due to SST assimilation was greater near the surface, while the improvement due to SLA assimilation was relatively great in the subsurface. The results after the assimilation of both SLA and SST were much better than those only assimilated one kind of dataset, but the difference due to the assimilation order of the two kinds of datasets was not significant.

Keywords Earth system model, Ocean satellite data, Ensemble adjustment Kalman filter, Data assimilation

Citation: Chen H, Yin X Q, Bao Y, Qiao F L. 2016. Ocean satellite data assimilation experiments in FIO-ESM using ensemble adjustment Kalman filter. Sci China Earth Sci, 59: 484−494, doi: 10.1007/s11430-015-5187-2

1. Introduction

Ocean observations have increased greatly thanks to the development of ocean satellites in recent decades. Many real-time or near-real-time products derived from satellite observations have been widely used in the study of large- and meso-scale oceanic processes. The oceanic datasets derived from satellite observations consist of sea surface temperature (SST) and sea surface height (SSH)/sea level anomaly (SLA), among others. The state of ocean in three dimensions cannot be examined directly using these satellite datasets because the observations are about the sea surface. Data assimilation combining a numerical model with observations can provide a better picture of realistic ocean state. Many studies (Ezer and Mellor, 1994; Yin et al., 2010, 2012; Zhang and Rosati, 2010; Ratheesh et al., 2012) pointed out that data assimilation improves model results of the ocean and provides better initial conditions for ocean forecast and climate prediction.

The increasing ocean observations have promoted the development and application of data assimilation, though new challenges need to be dealt with for proper use of these datasets in assimilation. The datasets derived from multi-

*Corresponding author (email: qiaofl@fio.org.cn)

satellite observations, such as SST and SLA, have different error characteristic. The key issues for data assimilation of ocean satellite observations are how to project the information observed at the sea surface onto subsurface (Haines, 1991; Ezer and Mellor, 1994), and how to effectively use these datasets to improve ocean and climate modeling. There were many studies focused on assimilating ocean satellite observations into numerical models. For example, Ezer et al. (1997) studied data assimilation in the Gulf Stream region and pointed out that assimilating both SST and SSH provided a result superior to that of only assimilating a single kind of dataset. Yin et al. (2010) assimilated the observations derived from satellite altimeters into a global general circulation model using a projection method, and found that the errors were significantly reduced. Ratheesh et al. (2012) studied the assimilation of SST and SLA in a regional circulation model of the Indian Ocean using a projection based on the correlation between SST/SLA and subsurface temperature; and their results also indicated that the assimilation of both datasets led to much better results. However, these studies were mostly performed in ocean circulation models only and used the Optimal Interpolation in which the covariance of the background errors did not change with time. An ocean model without coupling with other components is unable to well simulate climate change, an increasing concern of the public, especially when involving the tropical oceans where air-sea interaction is always intensive. In an ocean model without coupling, the surface forcing is given externally and there is no feedback at the air-sea interface. As a result, the ocean model is unable to reasonably simulate the spatial pattern and decadal variation in the tropical regions. In contrast, a coupled climate model considers more complete air-sea interaction processes, and therefore more information from observations could be absorbed during data assimilation by such a model (Zhang et al., 2014).

Ensemble Adjustment Kalman Filter (EAKF; Anderson, 2001) based on Ensemble Kalman Filter (EKF; Evensen, 1994) has been one research focus in recent years. In this method, perturbing observations in the traditional EKF is avoided and its performance is good even with a smaller ensemble number (Evensen, 2003). The background error covariance in EAKF is calculated by ensemble samples, which cause the covariance to vary with time, and its spatial and temporal evolution is decided by the dynamics of the numerical model itself. This ensures the covariance matrix can well capture the relationship among various physical processes. On the other hand, the computational cost of EAKF is greatly reduced because it uses a linear operator derived by the singular value decomposition of covariance matrix to update the ensemble samples, rather than using the gain matrix in traditional EKF.

In recent years, EAKF has been successfully applied in the Modular Ocean Model (Zhang et al., 2007), Princeton Ocean Model (Yin et al., 2010), Weather Research Forecast (Lei et al., 2012), and other ocean or atmospheric circulation models, and climate models. Zhang et al. (2007) designed a data assimilation system using EAKF for a fully coupled climate model and successfully reconstructed the variability and trends of twentieth-century ocean heat content in most regions. Karspeck et al. (2013) assimilated the temperature and salinity datasets from the World Oceanographic Database 2009 (WOD09) into the ocean component of the Community Climate System Model version 4 (CCSM4); their results showed significant improvement in the regions of boundary currents and the upper 1000 m. In general, data assimilation of a complex climate model using EAKF is more difficult in terms of technique and requires more computation resource. As a result, such studies are limited.

In this study, EAKF was implemented in the First Institute of Oceanography-Earth System Model (FIO-ESM). Two types of ocean satellite datasets (SLA and SST) were assimilated in this model, and four assimilation experiments were carried out to evaluate the effects of using different kinds of datasets in the assimilation and their orders in the assimilating process.

2. Ocean satellite data assimilation experiments

2.1 Brief introduction to FIO-ESM

Ocean surface wave plays an important role in an earth climate system and is an important part of a climate model (Hasselmann, 1991). However, surface wave is not included in most coupled climate models because it is considered as a small-scale process with a time scale quite different from climate change time scale.

Based on the non-breaking wave theory proposed in Yuan et al. (1999) and Qiao et al. (2004, 2010), a coupled climate model named FIO-ESM was developed. The FIO-ESM is the first model that includes surface waves. The model participated in the Climate Model Intercomparison Project Phase 5 (CMIP5). Some recent studies on the assessment of CMIP5 models showed that FIO-ESM has a good capability of simulating the mean SST state, Asian Monsoon, arctic sea ice, and other aspects of the climate system (Shu et al., 2013; Song et al., 2013; Sperber et al., 2013; Zhou et al., 2014).

The FIO-ESM includes five model components: the atmosphere model is CAM3.0 (Community Atmosphere Model version 3.0), the land-surface model CLM3.5 (Community Land Model version 3.5), the sea-ice model CICE4 (Los Alamos sea ice model version 4.0), the ocean circulation model POP2.0 (Parallel Ocean Program version 2.0), and the surface-wave model developed by the Key Lab of Marine Science and Numerical Modeling (MUSNUM). These components are coupled through Coupler6 developed by the National Center for Atmospheric Research (NCAR). The horizontal resolution of the atmosphere model is T42 (about

2.875°) with 26 layers in the vertical. The horizontal resolution of the land-surface model is the same as that of the atmosphere model. The horizontal resolution of the ocean circulation model is 1.1°×0.3° to 1.1°×0.5° with 40 layers in the vertical. The horizontal resolution of the sea-ice model is the same as that of the ocean circulation model. The horizontal resolution of the surface-wave model is 2°× 2°, with a resolution of 30° for wave direction. In the coupling procedure, data exchange between the coupler and the model components, including atmosphere, land surface, and sea ice, is carried out every hour; the data exchange between the coupler and the ocean circulation model is carried out every 24 hour; and the data exchange between the coupler and the surface-wave model is carried out every 6 hour.

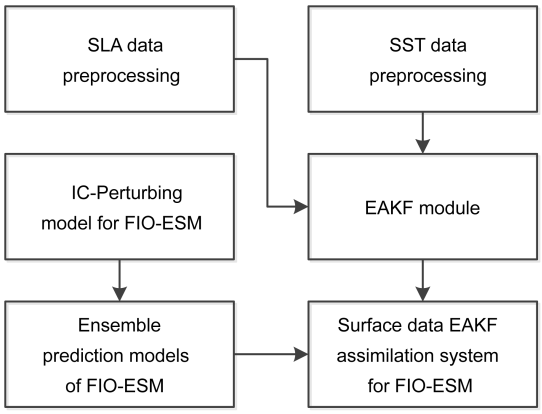

Figure 1 Flowchart of EAKF data assimilation system for FIO-ESM.

2.2 Designs of data assimilation system and experiments

The satellite data assimilation system of FIO-ESM consists of six components as shown in Figure 1. The SLA data preprocessor is designed to deal with SLA data, including unit conversion and quality data selection. During the quality data selection, the data that cannot pass the spatial gradient check is rejected. The SST data preprocessor is used to deal with SST data; and abnormal SST data is rejected before data assimilation. The paralleled EAKF module is developed following the method in Yin et al. (2012). In this study, all the variables of currents, temperature and SSH in the ocean circulation model are updated during the assimilation of SST and/or SLA.

About the generation of ensemble initial conditions (ICs), there are many attempts in the literature. For example, Zhang et al. (2005) used the restarts in different years as the ensemble ICs; and Feng et al. (2014) employed the Nonlinear Local Lyapunov Vectors to generate the ensemble ICs. In this study, the ensemble ICs were generated by a tiny-perturbing method. This method is simple to implement; and the dynamic relationship of variables in the model can be well maintained and the imbalance due to the perturbation on the ICs significantly reduced. Here, only the ocean temperature in three dimensions is perturbed, which can be expressed by the following formula:

$$T_{i,j,k}^{\text{pert}} = \left(1+\alpha\beta_{i,j,k}\right)T_{i,j,k}^{\text{init}}, \quad (1)$$

where α is a small value equal to 10^{-3}, and β is a random number within the range of (–1, 1). For different model runs, different random seeds are used for different ensemble samples to generate the random number at each model grid. The subscripts i, j and k are the indices of the model grid, and the superscripts 'pert' and 'init' represent the state before and after perturbation, respectively.

An ensemble of ICs (10 members) was obtained through the above method; and the ensemble prediction model is set up by starting FIO-ESM from each of these ICs. After running the ensemble model for two years, the spread tends to be stable and reaches 0.1–1.0 °C at the ocean surface and about 0.01°C at 1000 m. The following experiments use the ensemble outputs (after 2-year integration) as the ensemble ICs.

Five experiments in Table 1 have been conducted in this study. The control experiment (CTL) is an ensemble run of FIO-ESM, which is used for comparison with assimilation experiments. There are four assimilation experiments, of which AssimSLA and AssimSST are two experiments that assimilate only SLA or SST. The other two experiments assimilate both SLA and SST but in different orders. The experiment ran from January 1 to December 31, 2000, and the data assimilation was performed daily (at 00∶00 UTC). To avoid model overflow due to data assimilation, the adjustments of all the variables are not added directly; rather, They are added to FIO-ESM gradually at each time step, and the time scale of this procedure is set to 5 days. In addition, the localization used in Yin et al. (2010) is performed to reduce computational cost and to avoid pseudo covariance. The radius of this localization is set to 2° horizontally and 200 m vertically.

2.3 Data

The daily-averaged SLA data used for data assimilation was from the Archiving, Validation and Interpretation of Satellite Data in Oceanography (AVISO). This SLA data covers the global oceans with the horizontal resolution of 1/3°×1/3° (Ducet et al., 2002). The gridded product contains near-real-time and delayed-time versions, and the latter one is used in this study. The gridded product contains near-real-time and delayed-time versions, and the latter is used in this study.

The daily-averaged SST data is provided by the Climate Data Center of the National Oceanic and Atmospheric Administration (NOAA). This dataset is derived from meteorological satellites of NOAA-AVHRR (Advanced Very High Resolution Radiometer) and AMSR (Advanced Microwave

Table 1 List of experiments

Experiment	Data assimilated	Order	Icon in figures
CTL	None		No Assim
AssimSLA	SLA		Assim.SLA
AssimSST	SST		Assim.SST
AssimSLASST	SLA, SST	SLA first	Assim.SLA+SST
AssimSSTSLA	SST, SLA	SST first	Assim.SST+SLA

Scanning Radiometer), with the horizontal resolution of 1/4°×1/4° (Reynolds et al., 2007).

The data used in this study to evaluate the experiments include the temperature and salinity fields of EN3 produced by the Hadley Centre of the UK Met Office. This dataset is an objective analysis of temperature and salinity profiles of World Oceanographic Database 2005 (WOD05), Global Temperature Salinity Profile Program (GTSPP), Argo and Arctic Synoptic Basin-wide Observations (ASBO). The objective analysis of EN3 has a horizontal resolution of 1°×1° and 42 vertical layers. During the objective analysis, strict quality control was performed on the original observations of temperature and salinity profiles. More details about these processes can be found in Ingleby and Huddleston (2007).

3. Experiment results

3.1 Overall comparison

All the monthly-mean results of ocean temperature and salinity from different experiments are first ensemble-averaged and then interpolated onto the grids of EN3 dataset for comparison. Figure 2 shows the statistical absolute error of temperature and salinity in the upper 1000 m of CTL, respectively, in the horizontal and vertical directions. It can be seen that the temperature errors in most regions are less than 1°C (Figure 2(a)). The temperature errors are slightly larger in the regions around the equator, the Arabian Sea, the east coast of the equatorial Pacific, and the North Atlantic. The largest temperature error appears in the convergence region of the Labrador Sea, Norwegian Sea and Greenland Sea in the North Atlantic Ocean. Near 40°S of the Indian Ocean south of Australia, there is a belt of larger temperature error relative to that of the other regions of the Southern Ocean. The errors of salinity at depths shallower than 1000 m (Figure 2(b)) have a similar error distribution as those of temperature. The salinity errors are less than 0.2 psu in most regions and maxima are located in the North Atlantic and the east coast region of the Pacific. The temperature and salinity errors of CTL in the vertical direction are given in Figure 2(c). At the depths shallower than 100 m, the temperature error increases with depth, and the maximum reaches 1.55°C at about 120 m. Between the depths of 120 and 300 m, this error decreases with depth, while it increases between 300 and 600 m. Another extreme value of about 1.40°C is at about 600 m, and the temperature error rapidly decreases from 600 to 1000 m. The vertical change of salinity error (Figure 2(d)) is comparatively simpler than that of temperature, and the maximum is 0.62 psu at the surface. The temperature and salinity errors below 1000 m are negligibly smaller (not shown).

Figure 3 gives the time series of absolute errors in temperature and salinity of all the experiments. These errors are calculated for the depths shallower than 1000 m. The red line with dots in Figure 3(a) represents the result of CTL. It shows that the maximum temperature error occurs in February, decreases with time, and its value in December is 1.35°C. The salinity error in Figure 3(b) has the maximum in August, reaching 0.30 psu, and has the minimum in May. From the spatial and temporal distributions of temperature

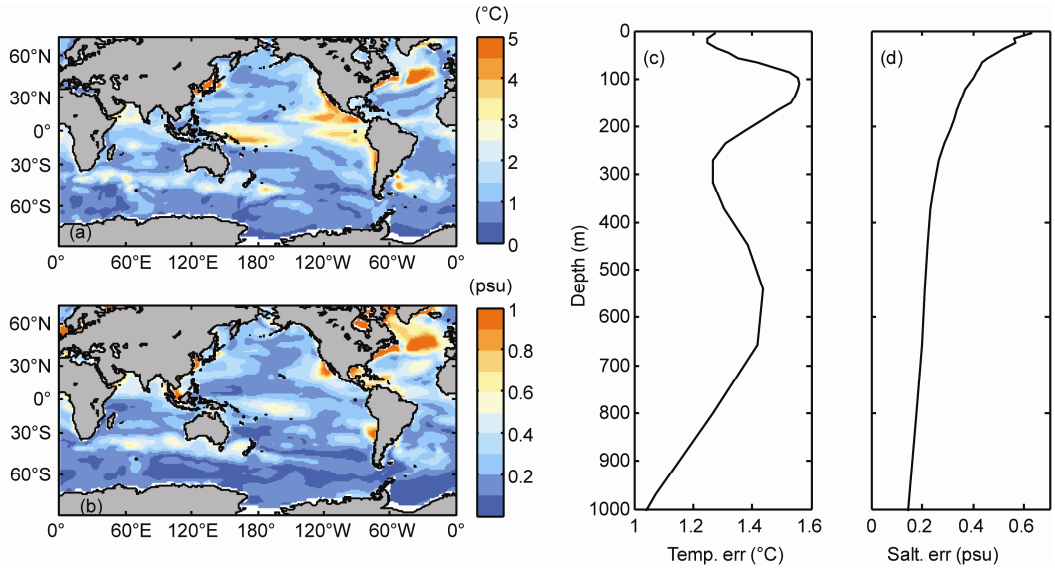

Figure 2 Horizontal/vertical differences of temperature ((a)/(c)) and salinity ((b)/(d)) in CTL at the depths shallower than 1000 m.

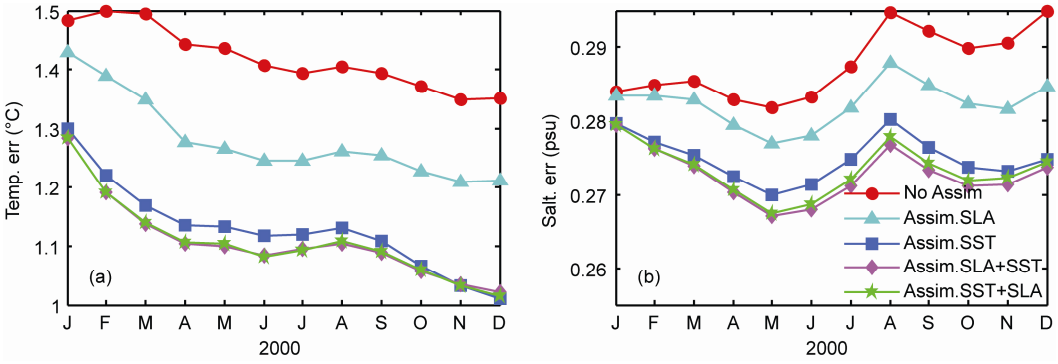

Figure 3 Simulated differences of temperature (a) and salinity (b) in each month. The red curve is for CTL, cyan curve is for Assim.SLA, blue curve is for Assim.SST, magenta is for Assim.SSTSLA, and green curve is for Assim.SLASST.

and salinity errors of CTL, we conclude that the ocean component of FIO-ESM is fairly reliable in terms of performance, but the differences between actual ocean observations and data assimilation outputs imply further improvement is needed.

The other four curves in Figure 3 are the temperature and salinity errors of the assimilation experiments. Overall, these errors are smaller than corresponding errors in CTL: the two experiments that assimilate both SLA and SST have the best performance, and the result of AssimSST is better than that of AssimSLA. This comparison indicates that the assimilation of both SST and SLA in FIO-ESM improves the simulation of the ocean model.

In order to examine the effects of data assimilation, these assimilation experiments are divided into two groups: one for the two experiments that only assimilates single kind of data (AssimSLA and AssimSLA), and the other for the two experiments assimilating both SST and SLA but in different orders (AssimSLASST and AssimSSTSLA). This categorization helps the analysis in following subsections where the effects of assimilating one single kind of data vs. two kinds are compared. Considering that the main improvement of data assimilation in FIO-ESM is located at the depths shallower than 1000 m, the following analysis will focus on the upper 1000 m.

The simulated differences between the CTL and four assimilation experiments are compared to indicate assimilation effects using the absolute error of CTL minus the absolute error of each of the four assimilation experiments. If the difference value is positive, it means the simulated biases are reduced after data assimilation. The simulated difference values are all positive in the upper 1000 m, and Figure 4 shows the reduced error due to data assimilation at depths shallower than 500 m.

3.2 Individual data assimilation experiments

The results of temperature in Figure 4(a) indicate the reduced error of AssimSLA reaching a maximum of about 0.25°C at 100 m. This error reduction decreases with depth in AssimSST, with its maximum (about 0.61°C) at the surface, which is about three times larger than that of AssimSLA. At the depths shallower than 200 m, the effect of AssimSST is better than that of AssimSLA; but the improvement between 200 and 300 m is larger in AssimSLA than in AssimSST. The improvements are similar in the depth range of 300–500 m. From the above discussions, we can see that SLA and SST datasets are more effective in the upper ocean; but the depths of maximum improvement are different. For the SLA assimilation, this depth is located at the subsurface (about 100 m), while for the SST assimilation it is located at the surface.

The differences in the horizontal distribution are checked using the absolute errors in temperature and salinity at each grid point shallower than 1000 m. Take temperature as an example, a scalar is defined as follows,

$$Absdif(i,j)=\frac{1}{N}\sum_{\substack{t=1,12\\ d(k)\leqslant 1000m}}\left|T^{\mathrm{CTL}}_{i,j,k,t}-T^{\mathrm{o}}_{i,j,k,t}\right| -\frac{1}{N}\sum_{\substack{t=1,12\\ d(k)\leqslant 1000m}}\left|T^{\mathrm{Assim}}_{i,j,k,t}-T^{\mathrm{o}}_{i,j,k,t}\right|, \quad (2)$$

where the superscript 'CTL' stands for the control experiment, 'Assim' stands for assimilation (experiment), and 'o' represents the observation. The subscripts '*i*', '*j*', '*k*', and '*t*' denote the spatial and temporal grid points, respectively; $d(k)\leq 1000$ m indicates the depth is shallower than 1000 m. Eq. (2) denotes the difference of absolute error between CTL and a data assimilation experiment. If *Absdif* >0, it means the absolute error in the assimilation experiment is smaller than that in CTL and the data assimilation has reduced the model error.

Figure 5 shows Absdif of temperature and salinity for the two experiments that only single type of data (SLA or SST) is assimilated. The regions with *Absdif* greater than zero are shaded, meaning the model error is reduced after data assimilation. In general, the temperature and salinity errors in most areas of the global ocean are reduced by data assimilation, and the pattern of *Absdif* is consistent with the distribution of absolute errors in CTL. This indicates that the EAKF assimilation system of FIO-ESM has improved

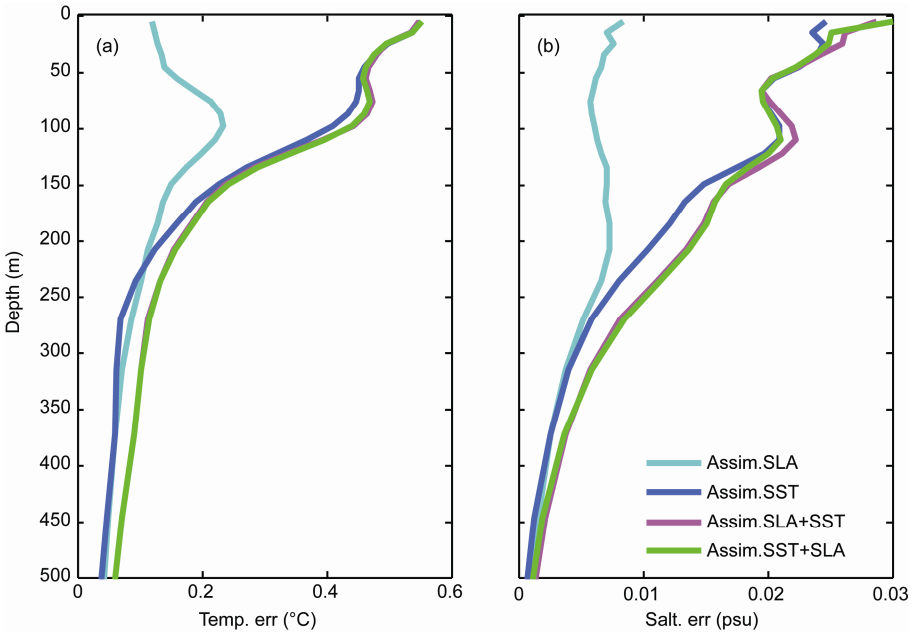

Figure 4 Differences of absolute errors in temperature/salinity (left/right: cyan for Assim.SLA; blue for Assim.SST; magenta for Assim.SSTSLA; green for Assim.SLASST) between each assimilation experiment and CTL at the depths shallower than 500 m.

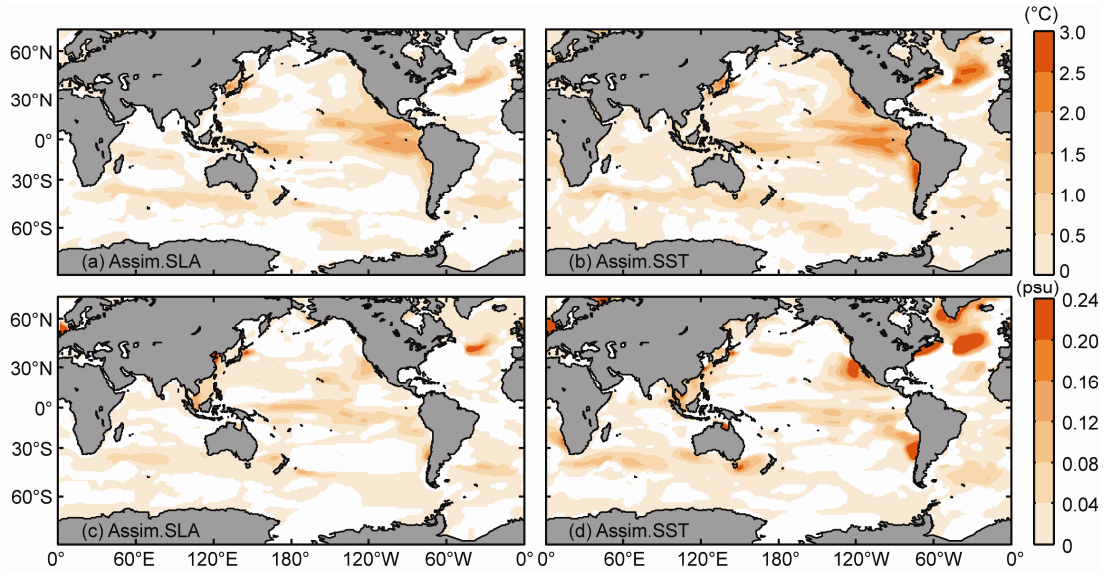

Figure 5 Horizontal distributions of Absdif in AssimSLA (left) and AssimSST (right).

model performance. Comparison of Figure 5(a) and (b) shows that the area of temperature error reduction in AssimSST is significantly larger than that in AssimSLA, and the value of *Absdif* in AssimSST is also larger than that in AssimSLA according to the contour levels. The maximum *Absdif* in AssimSLA is located in the eastern equatorial Pacific with a value of about 2°C, while that in AssimSST is located in the North Atlantic, with a value of about 3°C. Comparing Figure 5(c) and (d), we can see that the improved area and extent in salinity in AssimSST are much larger than those in AssimSLA. The white space in Figure 5 represent where *Absdif*<0, which means the simulated temperature or salinity errors are larger. The values of minimum *Absdif* for temperature in Figure 5(a) and (b) are around –0.25°C, and the minimum values of *Absdif* for salinity in Figure 5(c) and (d) are around 0.02 psu. The areas of negative *Absdif* are significantly smaller than those of positive *Absdif*. Therefore, both AssimSLA and AssimSST have reduced the simulation errors at the depths shallower than 1000 m, and the effect of AssimSST is better than that of AssimSLA in general.

The above analysis shows that error reductions in tem-

perature and salinity are different in the vertical and horizontal directions when different variable is assimilated. The results in Figures 4 and 5 show that the effect of SST assimilation is better than that of SLA assimilation. In order to examine the differences of these experiments in more detail, the absolute errors in temperature and salinity at different depths are calculated for each experiment as well as for CTL. The left panels of Figure 6 are the evolutions of temperature errors at the depths of 50, 100, 300, and 500 m, where the curves with different colors represent different experiments, respectively. At the depths of 50 and 100 m, the temperature errors in AssimSST are smaller than those in AssimSLA, but the temperature errors in AssimSLA become smaller than those in AssimSST during May to December. Similar results can also be found in salinity errors presented in the right panels.

Figures 7 and 8 are horizontal *Sindif* values for temperature and salinity at different depths of AssimSST and AssimSLA, respectively. *Sindif* is defined as the absolute error in AssimSST minus the absolute error in AssimSLA, see in eq. (3). If *Sindif* is greater than zero, it means the error in AssimSLA is relatively smaller. In Figures 7 and 8, negative *Sindif* is shaded in cold colors, while positive *Sindif* is shaded in warm colors. Figure 7 shows that the areas with cold colors reduce gradually with depth, while the areas with warm colors increase with depth. This indicates that the effect of SLA assimilation becomes relatively larger at subsurface, especially in the North Pacific Ocean. This result is consistent with the conclusion based on Figure 6, namely, the performance of SLA assimilation is superior to that of SST

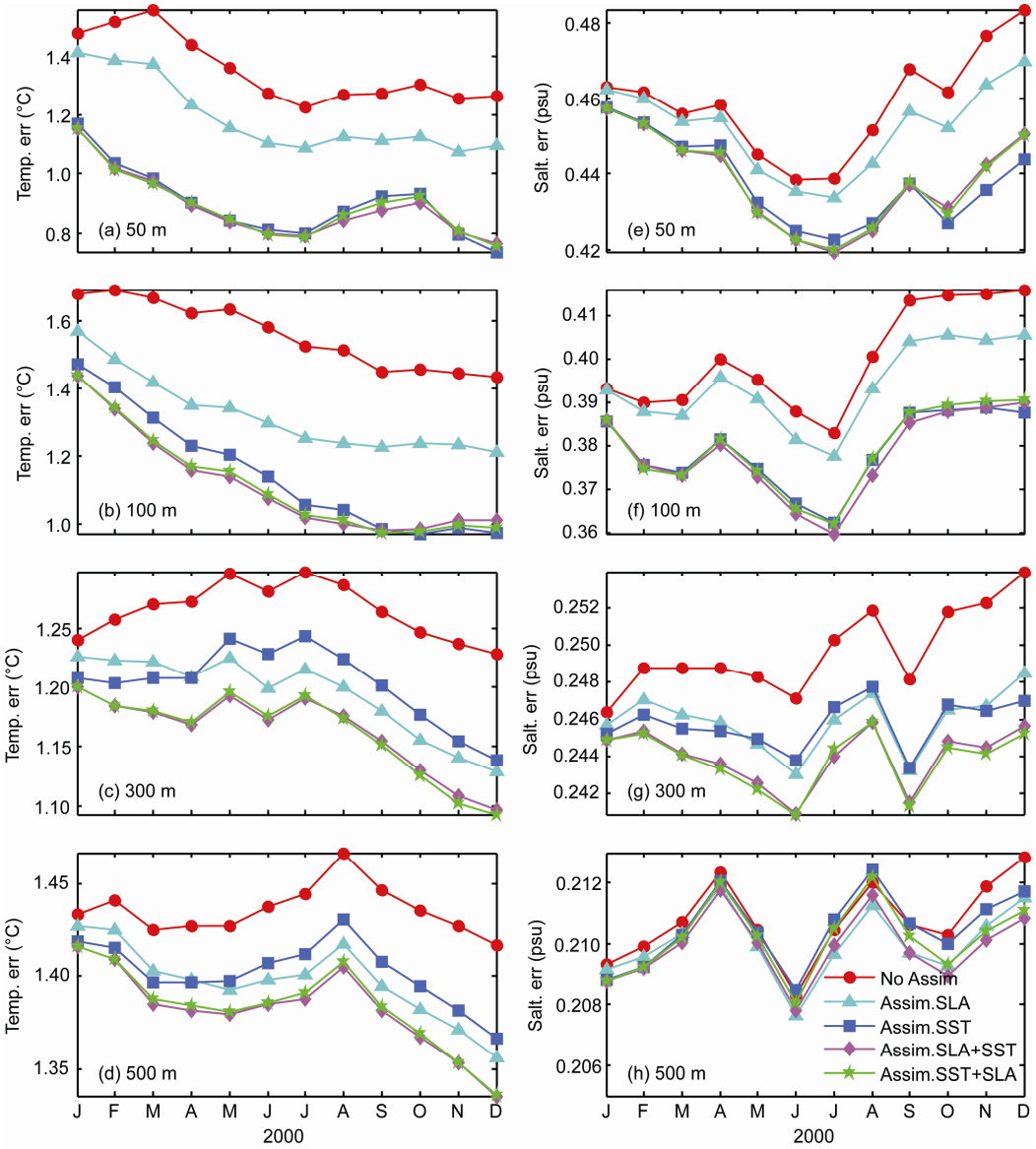

Figure 6 Simulated differences of temperature (left) and salinity (right) over time at depths of 50, 100, 300, and 500 m for all experiments (five colors are the same as in Figure 3).

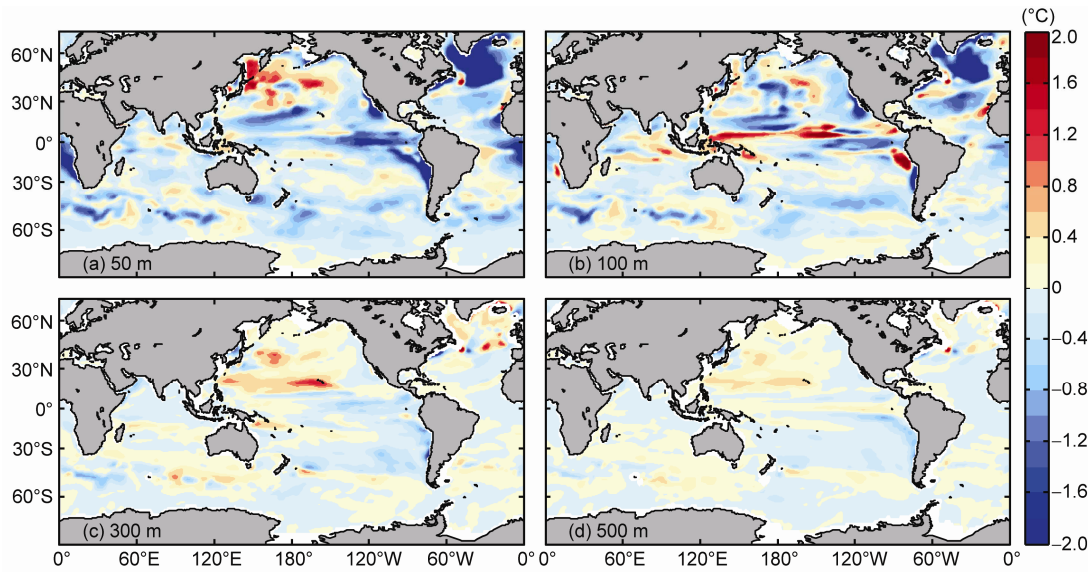

Figure 7 Simulated differences of temperature between AssimSST and AssimSLA at depths of 50, 100, 300, and 500 m.

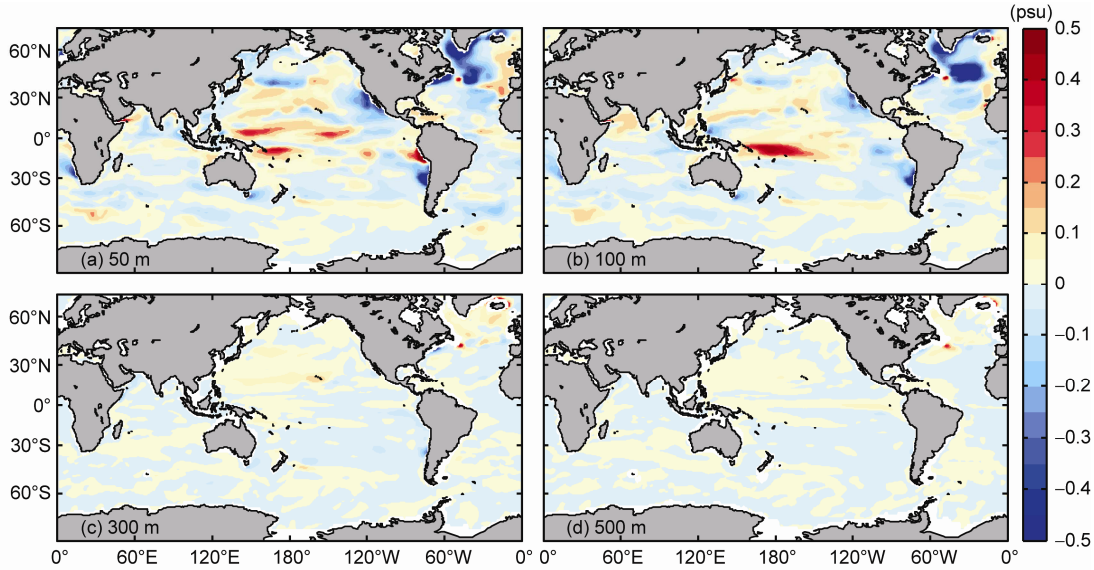

Figure 8 Same as Figure 7, except for salinity.

assimilation at 300–500 m.

$$Sindif = ABE_{\mathrm{AssimSST}} - ABE_{\mathrm{AssimSLA}}. \quad (3)$$

Similar to the study by Ezer and Mellor (1997), the maximum correlation coefficients between temperatures at different depths and SST are located near the surface, but the maximum correlation coefficients between temperatures at different depths and SLA are located at the subsurface.

Sindif for salinity (Figure 8) indicates similar results. The areas with red colors at 100 m are bigger than those at 50 m, but this increment trend with depth is relatively small for salinity errors. Through the comparison of Figures 6–8, we conclude that the effect of SST assimilation, overall, is better than that of SLA assimilation, but is not always at all depths; rather, the SLA assimilation is better than the SST assimilation at the subsurface.

Figure 9 shows error reductions in temperature and salinity along the equatorial section by data assimilation compared with CTL, that is, the absolute error in an assimilation experiment minus the absolute error in CTL. The differences of temperature errors are given in Figure 9(a) and (b), and the differences of salinity errors are given in Figure 9(c) and (d). The shading with warm colors in Figure 9 means the absolute errors are reduced after data assimilation. Comparing Figure 9(a) and (b), we can see that the absolute errors in AssimSLA are smaller than those in AssimSST at the depths of 300–1000 m. A comparison of different salinity

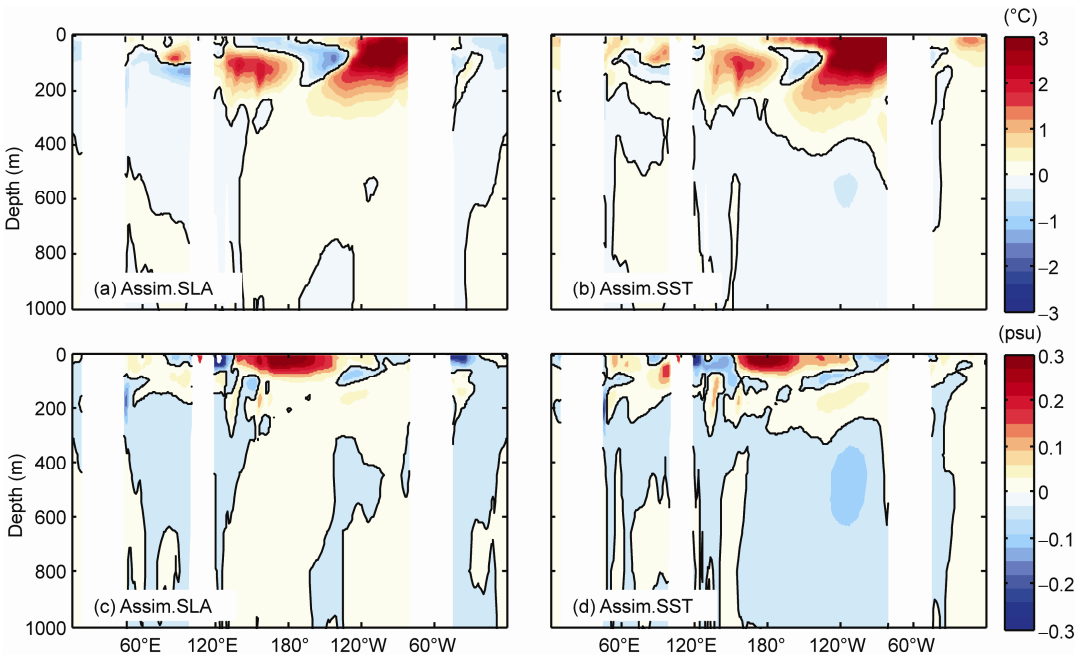

Figure 9 Simulated differences of temperature ((a), (b)) and salinity ((c), (d)) between each assimilation experiment and CTL along the equatorial section.

errors in Figure 9(c) and (d) indicates similar results. These comparisons confirm that the distribution of the correlation between SLA (or SST) and temperature is a key factor for improving the performance of data assimilation. The correlation between temperature and SST (SLA) has the maximum value at the surface (subsurface), suggesting different performances in the vertical direction when different kinds of datasets are assimilated.

Physically, the typical feature of temperature structure varying with depth in most regions of the ocean can be characterized as follows: the vertical variation is always small in the upper layers, and the temperature changes sharply near the thermocline, followed by a weak variation with depth in the deep ocean. The variation near the thermocline has an important contribution to the dynamic height, which causes the correlation between SLA and temperature to have a high value at the subsurface. On the other hand, the variation of SLA is affected by two main factors, horizontal movement and the baroclinic structure of the ocean. The analysis of the correlation of SSH and temperature in Zhang et al. (2013) had a similar viewpoint. That the correlation between SST and temperature is reduced with depth and that the correlation between SLA and temperature has a maximum value around the depth of 100 m are the reasons for the different performances of the individual assimilation experiments at different depths.

In conclusion, the assimilation of either SLA or SST improves the simulation results in FIO-ESM. Their maximum effects are located at the subsurface and near the surface, respectively. The overall performance of the SST assimilation is better than that of the SLA assimilation.

3.3 Joint data assimilation experiments

Figures 3, 4 and 6 show that the data assimilation experiments using both SLA and SST have an advantage over the data assimilation experiments using only one kind of data. In Figure 3, the temperature and salinity errors in AssimSSTSLA and AssimSLASST are all smaller than those in the other two experiments. The maximum error reductions with respect to CTL are 0.35ºC for temperature and 0.02 psu for salinity, but the differences between each of the two experiments that assimilate both SLA and SST and CTL are smaller. Comparing the temperature error reduction with respect to CTL in the vertical (Figure 4(a)), the difference is small in the upper 500 m. At the depths shallower than 150 m, the reduction of salinity error in AssimSLASST (Figure 4(b)) is slightly more than that in AssimSSTSLA, while they are very close in the depth range of 150–500 m. In Figure 6, the errors in temperature and salinity from the two joint data assimilation experiments are all very similar to those from AssimSST at 50 m, but they become smaller than those from AssimSST at 100 m, and are even smaller at 300 and 500 m. This indicates the data assimilation using both datasets leads to more improvement in the depth range of 300–500 m than the experiments only assimilating one kind of data. The results from the assimilation experiments using both datasets have larger improved areas than those from AssimSST, and the difference due to the order of data assimilation (SLA first, or SST first) is very small. We can conclude that the data assimilation using both SST and SLA, regardless of the order, leads to further improved performance, and that all the advantages in assimilating one kind of data is well kept and the effect of data as-

similation is enhanced by using the second kind of data set.

Figures 3, 4 and 6 show that there is only small difference in the data assimilation using both datasets due to assimilating orders. To further examine this difference, the simulated difference of AssimSSTSLA and AssimSLASST along the equator is given in Figure 10. This difference is calculated from the absolute error in AssimSSTSLA minus that in AssimSLASST. Therefore, the positive value with warm colors means that the error is smaller in AssimSLASST, and the negative value with cold colors means that the error is smaller in AssimSSTSLA. In Figure 10(a), the area with warm color indicates the assimilation effect of AssimSLASST being better than that of AssimSSTSLA; similarly, the area with cold color means the assimilation effect of AssimSSTSLA being better. The salinity (Figure 10(b)) results are the same as the temperature results. The errors of AssimSLASST are much smaller than those of AssimSSTSLA below 200 m. A conclusion could be drawn that the difference of the joint data assimilation experiments is not significant; the improvement of AssimSSTSLA is slightly better above 200 m but is slightly worse below 200 m.

Comparing with CTL, all the results after data assimilation have smaller errors, and the experiments that assimilate both SST and SLA have better performances than those that assimilate only one kind of data.

4. Conclusion and discussion

Based on the coupled model of FIO-ESM and EAKF method, four data assimilation experiments were carried out using SLA and/or SST datasets derived from satellite observations, in addition to the control experiment that has no data assimilation. The four assimilation experiments were analyzed to reveal the effects from different kinds of datasets and different assimilating orders if more than one kind of data was adopted. All the experiment results were compared with the objective analysis dataset of EN3.

Different from the ocean model without coupling, FIO-ESM is a coupled model with air-sea interaction. After ocean data assimilation, the subsequent responses of the atmosphere feeds back to the ocean through air-sea interaction. The relationships among variables are maintained during the assimilation in the coupled model. This is important for simulation and prediction (Zhang et al., 2014). And the multi-variable adjusting scheme in EAKF can make it.

Comparison of assimilation performances showed the data assimilation system of FIO-ESM is reliable, and indicated that assimilating both SST and SLA can improve the performance of the ocean model, especially at the depths shallower than 1000 m. For the effects located at different depths due to assimilating SST or SLA, the model output is improved near the surface after SST assimilation and at the subsurface after SLA assimilation. The joint data assimilation of both SST and SLA improves more the simulation results than only assimilating one kind of data; and the order of the two kinds of datasets assimilated is insignificant.

There are five component models in FIO-ESM, including ocean, atmosphere, ice, land surface, and ocean surface wave. Only the results of the ocean after data assimilation were presented in this paper. The effects of data assimilation on other model components need to be carefully examined in future, and the influence of the coupling process due to data assimilation needs to be further assessed.

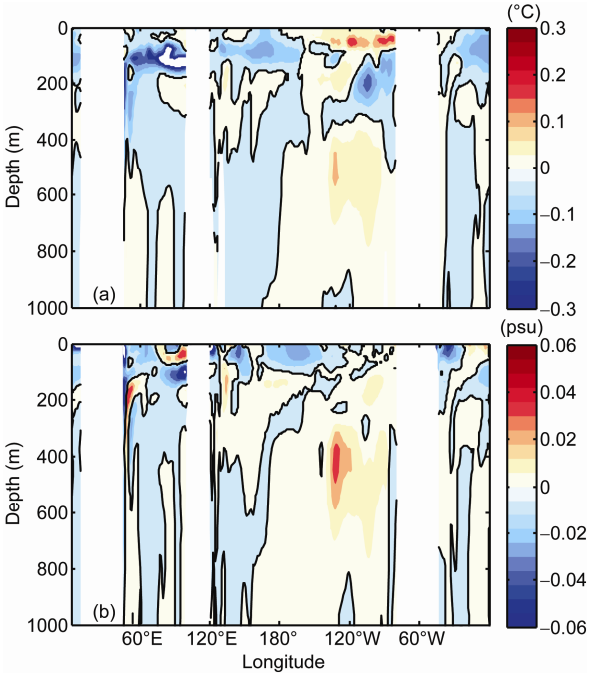

Figure 10 Simulated differences of temperature (a) and salinity (b) between the two joint assimilation experiments along the equatorial section.

Acknowledgements *This study was supported by the National Natural Science Foundation of China-Shandong Joint Fund for Marine Science Research Centers (Grant No. U1406404), the Public Science and Technology Research Funds Projects of Ocean (Grant No. 201505013), and the Scientific Research Foundation of the First Institute of Oceanography, State Oceanic Administration (Grant No. 2012G24).*

References

Anderson J L. 2001. An ensemble adjustment Kalman filter for data assimilation. Mon Weather Rev, 129: 2884–2903

Ducet N, Le Traon P Y, Reverdin G. 2000. Global high-resolution mapping of ocean circulation form TOPEX/Poseidon and ERS-1and -2. J Geophys Res, 105: 19477–19498

Evensen G. 1994. Sequential data assimilation with a nonlinear quasi-geotropic model using Monte Carlo methods to forecast error statistics. J Geophys Res, 99: 143–162

Evensen G. 2003. The ensemble Kalman Filter: Theoretical formulation and practical implementation. Ocean Dyn, 53: 343–367

Ezer T, Mellor G L. 1994. Continuous assimilation of GEOSAT altimeter data into a three dimensional primitive equation Gulf Stream model. J Phys Oceanogr, 24: 832–847

Ezer T, Mellor G L. 1997. Data assimilation experiments in the Gulf

Stream region: How useful are satellite-derived surface data for nowcasting the subsurface fields? J Atoms Ocean Tech, 14:1379–1391
Feng J, Ding R Q, Liu D, Li J P. 2014. The application of nonlinear local Lyapunov vectors to ensemble predictions in the lorenz systems. J Atmos Sci, 71: 3554–3567
Hasselmann K. 1991. Ocean circulation and climate change. Tellus A, 43: 82–103
Haines K. 1991. A direct method for assimilating sea surface height data into ocean models with adjustments to the deep circulation. J Phys Oceanogr, 21: 843–868
Ingleby B, Huddleston M. 2007. Quality control of ocean temperature and salinity profiles-historical and real-time data. J Marine Syst, 65: 158–175
Karspeck A R, Yeager S, Danabasoglu G, Hoar T, Collins N, Raeder K, Anderson J, Tribbia J. 2013. An ensemble adjustment kalman filter for the CCSM4 ocean component. J Clim, 26: 7392–7413
Lei L, Stauffer D R, Deng A. 2012. A hybrid nudging-ensemble Kalman filter approach to data assimilation in WRF/DART. Q J R Meteorol Soc, 138: 2066–2078
Qiao F L, Yuan Y L, Yang Y Z, Xia C S, Ma J. 2004. Wave-induced mixing in the upper ocean: Distribution and application to a global ocean circulation model. Geophys Res Lett, 31: L11303, doi: 10.1029/2004GL 019824
Qiao F L, Yuan Y L, Ezer T, Xia C S, Yang Y Z, Lü X G, Song Z Y. 2010. A three-dimensional surface wave-ocean circulation coupled model and its initial testing. Ocean Dyn, 60: 1339–1355
Qiao F L, Song Z Y, Bao Y, Song Y J, Shu Q, Huang C J, Zhao W. 2013. Development and evaluation of an Earth system model with surface gravity waves. J Geophys Res, 118: 4514–4524
Ratheesh S, Sharma R, Basu S. 2012. Projection-based assimilation of satellite-derived surface data in an Indian Ocean circulation model. Mar Geod, 35: 175–187
Reynolds R W, Smith T M, Liu C, Chelton D B, Casey K S, Schlax M G. 2007. Daily high-resolution blended analyses for sea surface temperature. J Clim, 20: 5473–5496
Shu Q, Qiao F L, Song Z Y. 2013. The hindcast and forecast of Arctic sea ice from FIO-ESM (in Chinese). Acta Oceanol Sin, 35: 37–45
Song Y J, Qiao F L, Song Z Y, Jiang C F. 2013. Water vapor transport and cross-equatorial flow over the Asian-Australia monsoon region simulated by CMIP5 climate models. Adv Atmos Sci, 30: 726–738
Sperber K R, Annamalai H, Kang I S, Kitoh A, Moise A, Turner A, Zhou T. 2013. The Asian summer monsoon: An intercomparison of CMIP5 vs. CMIP3 simulations of the late 20th century. Clim Dyn, 41: 2711–2744
Yin X Q, Qiao F L, Yang Y Z, Xia C S. 2010. An ensemble adjustment Kalman filter study for Argo data. Chin J Oceanol Limn, 28:626–635
Yin X Q, Qiao F L, Yang Y Z, Xia C S, Chen X Y. 2012. Argo data assimilation in ocean general circulation model of Northwest Pacific Ocean. Ocean Dyn, 62:1059–1071
Yuan Y L, Qiao F L, Hua F, Wan Z W. 1999. The development of a coastal circulation numerical model: 1. Wave-induced mixing and wave-current interaction (in Chinese). J Hydrodyn Ser A, 14: 1–8
Zhang S Q, Harrison M J, Wittenberg A T, Rosati A, Anderson J L, Balaji V. 2005. Initialization of an ENSO forecast system using a parallelized ensemble filter. Mon Weather Rev, 133: 3176–3201
Zhang S Q, Harrison M J, Rosati A. Wittenberg A. 2007. System design and evaluation of coupled ensemble data assimilation for global oceanic climate studies. Mon Weather Rev, 135: 3541–3564
Zhang S Q, Rosati A. 2010. An inflated ensemble filter for ocean data assimilation with a biased coupled GCM. Mon Weather Rev, 138: 3905–3931
Zhang S Q, Chang Y S, Yang X S, Rosati A. 2014. Balanced and coherent climate estimation by combining data with a biased coupled model. J Clim, 27: 1302–1314
Zhang Z G, Zhang Y, Wang W, Huang R X. 2013. Universal structure of mesoscale eddies in the ocean. Geophys Res Lett, 40: 3677–3681
Zhou T J, Chen X L, Dong L, Wu B, Man W M, Zhang L X, Lin R P, Yao J C, Song F F, Zhao C B. 2014. Chinese contribution to CMIP5: An overview of five Chinese models' performances. J Meteorol Res, 28: 481–509